This is a repository copy of *Mechanical, thermal insulation, thermal resistance and acoustic absorption properties of geopolymer foam concrete*.

White Rose Research Online URL for this paper:
http://eprints.whiterose.ac.uk/90607/

Version: Accepted Version

Mechanical, thermal insulation, thermal resistance and acoustic absorption properties of geopolymer foam concrete (GFC)

Zuhua Zhang [a]*, John L. Provis [b], Andrew Reid [c], Hao Wang [a]*

[a] Centre of Excellence in Engineered Fibre Composites (CEEFC), Faculty of Health, Engineering and Sciences, University of Southern Queensland, Toowoomba, Australia. Email: Hao.Wang@usq.edu.au (first corresponding author); Zuhua.Zhang@usq.edu.au (second corresponding author)

[b] Department of Materials Science and Engineering, The University of Sheffield, Sheffield S1 3JD, United Kingdom. Email: j.provis@sheffield.ac.uk

[c] Halok Engineering Ltd. Brisbane, Queensland 4101, Australia. Email: Andrew.Reid@Haald.com.au

Abstract

This study reports the synthesis and characterization of geopolymer foam concrete (GFC). A Class F fly ash with partial slag substitution was used for GFC synthesis by mechanical mixing of preformed foam. The GFCs exhibited 28 day compressive strengths ranging from 3 to 48 MPa with demolded densities from 720 to 1600 kg/m^3 (105°C oven-dried densities from 585 to 1370 kg/m^3), with the different densities achieved through alteration of the foam content. The thermal conductivity of GFCs was in the range 0.15 to 0.48 W/m·K, showing better thermal insulation properties than normal Portland cement foam concrete at the same density and/or at the same strength. The GFC derived from alkali activation of fly ash as a sole precursor showed excellent strength retention after heating to temperatures from 100 to 800°C, and the post-cooling compressive strength increased by as much as 100% after exposure at 800°C due to densification and phase transformations. Partial substitution of slag for fly ash increased the strength of GFC at room temperature, but led to notable shrinkage and strength

1

loss at high temperature. Thin GFC panels (20 - 25 mm) exhibited acoustic absorption

coefficients of 0.7-1.0 at 40 to 150 Hz, and 0.1-0.3 at 800 to 1600 Hz.

Keywords: Alkali activated cement; Geopolymer; Foam concrete; Thermal insulation; Acoustic absorption; Thermal resistance

1. Introduction

The search for materials offering high thermal insulation has increasingly become a target of

the modern construction and building industry, as energy-efficiency of buildings in service has

become of ever increasing concern. Foam concrete is well known for its relatively low thermal

conductivity, usually 10 to 50% of that of normal dense concrete, depending on the designed

material density and composition [1-3]. This low thermal conductivity brings good thermal

insulation, and usually energy efficiency in operation. Recent developments in alternative

binders, and in engineering of products based on these binders, have led to the manufacture of

foam concrete using geopolymer as the binder [4]. Geopolymers are a complex class of

materials, principally manufactured through alkali hydroxide and/or silicate activation of a

reactive aluminosilicate, in particular calcined clays (metakaolin) or fly ash [5]. One of the

most attractive benefits of geopolymer materials is the reduced energy consumption and CO_2

emissions which are achievable compared to ordinary Portland cement [6]. The innovation of

geopolymer foam concrete (GFC) creates an approach of developing energy efficient materials

from material manufacturing to building operation, which seems to offer the possibility to be

eco-friendly across the whole life cycle.

GFC can be synthesized effectively by a chemical foaming technique [4]. Arellano Aguilar et al. [7] prepared GFCs based on alkali-activated metakaolin binders with Al powder as gas-releasing agent. The 28 d compressive strength of GFCs was in the range of 2 to 14 MPa for densities from 600 to 1200 kg/m^3. This strength is relatively high when compared with Portland cement-based foam concrete in a similar density range [8]. However, the thermal conductivity of the GFCs was high, from 0.49 to 1.22 W/m·K, and this was attributed to the high humidity in the GFCs and the quartz and cristobalite present in metakaolin [7]. Kamseu et al. [9] also prepared metakaolin-based geopolymer foams using Al powder as a foaming agent, and the resulting foams had low thermal conductivity (0.15-0.4 W/m·K). The thermal conductivities of the solid geopolymer binders synthesized by those authors increased with increasing Si/Al ratio [10], in agreement with previous research [11], which is related to the increased connectivity, the reduced porosity and the finer pore size distribution as the Si/Al ratio increases. Silica fume can also be used as the foaming agent in GFC production via an *in situ* foaming technique [12]. During sealed curing, free (reduced) silicon present in the silica fume will be oxidized by water, releasing hydrogen gas, which introduces bubbles into the geopolymer paste. Such products usually exhibit low thermal conductivity (0.22-0.24 W/mK) but also low strength (around 1 MPa), due to the extremely heterogeneous pore structure and large pore size [13, 14].

GFC can also be made using a mechanical pre-foaming technique. Zhang et al. [15] manufactured a series of GFCs using fly ash as the main aluminosilicate precursor by mechanical mixing with a preformed foam. The fly ash-based GFCs possessed dry densities from 850 to 950 kg/m^3 and compressive strengths of 4 to 9 MPa, depending on the type and dosage of alkali activator. Al Bakri Abdullah et al. [16] also manufactured GFC with fly ash by mixing pre-formed foam into geopolymer paste at a 2:1 volume ratio. The resulting GFCs reached 18 MPa under room temperature curing conditions at a density of 1660 kg/m^3.

The development of GFC is currently in the relatively early stages of technological maturity. Only limited information has been reported regarding the relationship between composition, structure and properties of this new material. Some special challenges related to this material require particular attention, such as understanding the differences between dense and foamed geopolymers [4]. This study has been conducted to investigate the key properties of GFCs, including compressive strength, acoustic absorption, thermal insulation and fire resistance. Understanding of these properties is useful for the widespread uptake of this new material.

2. Materials and Methods

2.1 Materials

The geopolymer binder was prepared using a Class F fly ash (Tarong, Australia) with partial substitution of a granulated blast furnace slag (Cement Australia Pty Ltd) as secondary calcium source. The chemical compositions of the fly ash and the slag were determined by X-ray fluorescence (Table 1). Fig. 1 shows their particle morphology, as observed using a JEOL JCM-600 Benchtop scanning electron microscope, for samples coated with gold. The majority of fly ash particles are in the range of 2-100 micrometers in diameter, and the slag seems to have more fine particles than the fly ash. The particle size distributions of the two solid materials were also determined using a Malvern Mastersizer 2000 (Fig. 2). The surface areas of the fly ash and the slag used are estimated by this method to be 0.64 and 0.69 m^2/g respectively. The activators used included an NaOH solution and a sodium silicate solution. The NaOH solution was prepared by dissolving NaOH pellets (99% purity, Taiwan Alum Chemical Industrial Co., Ltd.) in water to a concentration of 12 mol/L, and cooling to room temperature. The sodium silicate solution was D-Grade ^{TM} liquid sodium silicate (PQ Australia) with Ms (molar ratio

4

$SiO_2/Na_2O) = 2.0$ ($Na_2O = 14.7$ wt.%, $SiO_2 = 29.4$ wt.%). Distilled water was used throughout the experimental section. The foaming agent was a diluted aqueous surface active concentrate.

2.2 Methods

2.2.1 GFC manufacture

Two batches of GFCs (Table 2) were manufactured to examine the effects of slag substitution and foam dosage on the mechanical and thermal properties of the material. Due to the lack of standards available for GFC preparation, some Portland cement (PC) foam concrete specifications have been used as a reference baseline [17]. The fly ash and slag were dry-mixed for 5 min, then mixed with the NaOH solution, followed by the sodium silicate solution and additional water. At the end of paste mixing, foam was generated using an air pressure foam generator, weighed, and immediately transferred into the homogeneous geopolymer paste for final mixing for 1 - 2 min. Low speed mixing was used to avoid bubble breakage due to the high viscosity of the geopolymer paste. The fresh foamed mixtures were cast in ø53×105 mm and ø100×200 mm plastic molds, sealed with with plastic film wrap, cured at 40°C for 24 h, aged for 27 d at ambient conditions, and then demolded for testing and characterization.

2.2.2 Mechanical testing

The compressive strength of GFC was tested using an MTS universal mechanical testing instrument at a loading speed of 0.5 mm/min. A minor volume change after curing was noted; therefore the top surfaces of samples were all sanded carefully to be flat and parallel before testing. The weight, diameter and length of each sample were measured to enable calculation of demolded density (weight/volume). Dry densities of GFCs were also measured after drying the crushed specimens at 105±2°C in oven for 24 h, as per ASTM C495. For the strength and

5

density measurements, the mean values of four samples for each mixture are reported, and the standard deviations for each mix are reported as apparent errors.

2.2.3 Acoustic absorption

The acoustic absorption of GFC was evaluated in accordance with ASTM E 1050, using a modified impedance tube. The apparatus, described elsewhere [18], tests the sound absorption of acoustic insulating materials by using a vacuum pump behind the sample; the testing of GFC was performed under ambient air conditions. Cylindrical samples with diameter of 100 mm were cut into pieces with thickness of 20 and 25 mm, and sanded carefully on the surface to a diameter of 95 mm, which fit snugly into the specimen holder. The specimen holder was placed into the testing tube at one end, and the other end was the sound source. Along the tube were placed two microphones, which detected the sound wave pressure transmitted to the sample and the portion of the wave that was reflected. The complex reflection coefficient (R) at a particular frequency is determined by Eq.1:

$$R = \frac{e^{jkd_1} - Pe^{jkd_2}}{Pe^{-jkd_2} - e^{jkd_1}} \tag{Eq.1}$$

where j is $\sqrt{-1}$, k is the wave number, d_1 and d_2 are the distances between the specimen surface and the near and far active microphones respectively, and P is the ratio of sound pressure at the two active microphone locations.

The normal incidence acoustic absorption coefficient (α) is calculated by Eq.2:

$$\alpha = 1 - |R|^2 \tag{Eq.2}$$

To obtain precise measurements without influence from moulded or free end surfaces, samples were cut from the middle of each specimen. The two surfaces were cleaned with compressed

air to remove any particles that were blocking the foam voids. The frequency range tested was from 0 to 1600 Hz, which is limited by the fixed diameter of the impedance tube.

2.2.4 Thermal conductivity

The thermal conductivity of GFC was measured at ambient conditions using the transient plane source (TPS) method on a Hot Disk 2500 system. The samples were cut from GFC specimens with diameter 53 mm, to form discs with thickness of 15±2 mm. In order to ensure good contact between the TPS element and the sample surface, all samples were polished flat and parallel, and cleaned with compressed air. Fig. 3 shows two pieces used for one sample. For each geopolymer mixture, four replicate tests were conducted.

The humidity of the sample has an important impact on the measured thermal conductivity [11, 19]. Because drying at high temperatures for long periods may change the phases and/or microstructure of the geopolymer, a short drying period (6 h) at a moderate temperature (80°C) was adopted in this study. It was noted that the weight loss did not exceed 1% if they were dried for a further 6 h; the porous microstructure and the low thickness enabled this rapid drying of the samples at 80°C.

2.2.5 Thermal resistance

Thermal resistance of GFC was evaluated by measuring the strength and volume changes after exposure to high temperatures. Selected specimens were heated in an oven at a 10°C/min heating rate to 100°C and held for 4 h, then naturally cooled down to room temperature in the oven. Some were heated in a muffle furnace with a 10°C/min heating rate from room temperature to 400 and 800°C, held for 3 h, and allowed to cool down to room temperature in the furnace. The compressive strengths of GFCs before and after heating were tested using the MTS universal mechanical testing instrument as described in section 2.2.2. The linear

shrinkage of the heated specimens was also measured. Phase changes after heating were analyzed by X-ray diffraction (XRD) using an ARL 9900 Series X-ray workstation (Thermo Scientific) with Co Kα radiation, operated at 40 kV and 40 mA, with a step size of 0.02° and count time of 1 s/step from 8 to 80° 2θ.

3. Results and discussion

3.1 Compressive strength of GFC

Fig.4 shows the effect of slag substitution on the compressive strength of the GFCs produced in this study. At a constant foam dosage of 5% (mass ratio to solid precursor), the 100% fly ash GFC specimen F5S0 achieves 7.5 MPa at 28 d. By using 20% slag substitution for fly ash, the compressive strength of F5S20 increases to 12.6 MPa, while further slag substitution causes a slight loss of strength. The largely beneficial influences of slag addition on the strength development of fly ash-based geopolymers have been reported extensively in the literature [20-23]. The alkali-activated fly ash binder consists of sodium aluminosilicate gel (N-A-S-(H)) as the dominant phase, with residual embedded fly ash particles [5]. When calcium cations are made available by slag dissolution under geopolymerization conditions, there will be more calcium-rich aluminosilicates, mostly Al-substituted calcium silicate hydrates (C-A-S-H), formed [5, 23]. Homogeneous but XRD-amorphous phases with composition of N-C-A-S-H are also often observed in alkali-activated systems [22]. These phases with relatively high Ca/Si ratios (by the standards of geopolymerization reaction products, but not compared to Portland cement hydrates) are regarded as strengthening phases in geopolymer binders [20, 23]. In addition to the formation of calcium-containing products, the reaction extent of fly ash can be improved through blending with slag. When the alkali activator contains soluble silicate, the

calcium dissolved from the fly ash is able to form precipitates in the liquid phase, rather than on the fly ash surface, thus reducing hindrance of the dissolution of bulk particles [24]. The much higher reaction heat release rate for fly ash-based geopolymer mixes containing higher CaO or slag contents has been demonstrated [21, 25]. However, in the case of manufacturing GFC, slag substitution also changes the pore structure, due to the changes in rheology and setting time. The relationship between slag content and density (Fig. 4) shows that incorporation of 30% or more slag leads to reduced density. This implies that more bubbles are stabilized in the binder, giving a reduction in strength. Thus, the optimal slag substitution for this application is probably between 20 and 30%.

Fig. 5 shows the effect of foam dosage on the compressive strength of GFC, for a set of samples with a constant 30% slag substitution. The compressive strength of GFC is closely related to its density, both decreasing notably with the addition of up to 7% foam, and then more gradually beyond that point. The compressive strengths and densities of normal PC foam concretes are in the ranges 1 to 10 MPa and 360 to 1400 kg/m^3 respectively [4], but the strength performance has been shown to be improved by the addition of fly ash, e.g. to a density range of 650 - 1224 kg /m^3 with compressive strengths of 2 - 18 MPa [26]. Highly blended PC foam concretes which incorporated silica fume, fly ash and slag exhibited 710 - 1520 kg /m^3 and 4.2 - 23.7 MPa [27]. In comparison, the GFCs produced here have higher strengths at the same density. In the density range higher than 1000 kg /m^3, the GFCs are able to be used for semi-structural to structural purposes.

3.2 Thermal insulation

Fig. 6 presents the thermal conductivity and thermal diffusivity of GFC at room temperature. The thermal conductivity increases from 0.15 to 0.48 W/m·K when the dry density increases

from 585 to 1370 kg/m^3, as the foam dosage decreases accordingly. The thermal diffusivity was measured to be 0.27 - 0.34 mm^2/s, with a general increasing trend as a function of density. The thermal conductivity of GFC is in the same range as that of geopolymer foams derived from metakaolin with Al powder as the foaming agent [11]. The thermal conductivity of PC foam concretes has been observed to range from 0.15 to 0.6 W/m·K for densities between 400 and 1700 kg/m^3, across a variety of foaming or density-reduction methods [4]. At a density of 1000 kg/m^3, the GFCs have a thermal conductivity of 0.24 W/m·K, which is lower than the range reported for PC foam concretes, 0.3 to 0.5 W/m·K, depending on the composition, fillers and testing conditions [4]. This is attributed to the low level of chemically bound water in the geopolymer gel, providing a more discontinuous gel structure in these materials. The thermal diffusivity of GFC is much lower than that of fully dense PC concretes, which decreases creases from 1.2 to 1.1 mm^2/s as the hydration degree of cement increases from 0 to 1 (fully hydrated) [28]. The measured thermal diffusivities of the as-cured dense metakaolin-based geopolymers are between 0.24 and 0.26 mm^2/s [11], which are close to the results in the present study. The GFCs can thus be regarded as excellent thermal insulation building materials for their low thermal conductivity and relatively low thermal diffusivity.

3.3 Thermal resistance

The thermal resistance of GFC is evaluated here by measuring changes in strength and volume after high temperature exposure. Fig.7 presents the residual compressive strengths of GFCs after exposure at temperatures between 100 and 800°C. The compressive strengths of F5S0 and F5S30 both increase after heating at 100°C, but when exposed to 400 and 800°C, the two mix types exhibit different strength behaviors. F5S0, which is a purely fly ash-based foam and thus contains a solely aluminosilicate gel, maintains its strength at 400°C, and increases by

50% after heating to 800°C. The good compressive strength retention up to 400°C (actually slight increase in this study) was also observed in the dense 8 M NaOH-activated fly ash binder [29]; the remarkable strength increase of F5S0 at 800°C is in agreement with these reported results. Rickard et al. [30] also showed that the strengths of solid geopolymers increase after exposure to 1000°C, when low iron and low calcium-bearing fly ashes are used. In contrast, F5S30 decreases in strength by 40% at 400°C and 50% at 800°C, as its structure is much more disrupted by the loss of chemically bound water from the relatively calcium-rich gels formed through combined fly ash-slag activation. The better strength retention of Al-Si rich gels compared to calcium-containing gels was also observed in alkali-activated metakaolin/slag blends [31]. Substitution of slag by 20% metakaolin led to relatively larger strength loss upon heating than in the unblended binder, attributed to the dehydroxylation of Ca-containing products formed in these systems. It was also noted that the alkali-activated metakaolin binder (Al-Si rich gels) in that study gained some strength after exposure to 1000°C, while the slag blended binder did not [31].

The large strength loss in F5S30 is a consequence of both physical and chemical property changes, including volume, pore structure and phase decomposition. The volume change has caused cracks on the surfaces, which is linked to the strength loss, but is also the reason for the large variability in the post-heating testing results, as crack formation is a stochastic process and so induces cracks of different size in each replicate specimen. A large standard derivation in compressive strength after heating, such as the large errors indicated in Fig. 7, has also been found in other research [32, 33]. Fig. 8 shows the volumetric stability, expressed in terms of linear shrinkage, of the specimens after heating to different temperatures. The linear shrinkage increases directly with temperature in the heating range studied. Because dimensional measurements are taken after cooling of the specimens, the transient swelling/expansion peaks

11

seen in dilatometry analysis of fly ash geopolymer specimens [34, 35] are not seen here, as the expanded product collapses relatively rapidly.

From room temperature to 100°C, F5S0 and F5S30 show little shrinkage (-0.02 to -0.07%), which is consistent with results for dense inorganic polymers [35]. In this temperature region, only free water evaporates from the geopolymer foams. For metakaolin-based geopolymers, which contain relatively higher amount of evaporable water, the loss of free water may cause large shrinkage, and even visible cracks [36]. However, the dilatometric curves presented by Dombrowski et al. [37] do not show shrinkage when their dense fly ash-based geopolymer samples with varied amounts of $Ca(OH)_2$ were heated up to 100°C. Instead, their results show a 0.1% expansion for the samples under load and no shrinkage for the samples without load. Although some other dilatometric studies [38, 39] also showed a similar small expansion before 100°C, a certain extent of shrinkage is normally observed at 100°C when starting from as-cured (moist) samples [32, 34, 35, 40]. The small expansion before 100°C observed in some research is probably due to the thermal expansion properties of the solid geopolymer gel. Lemougna et al. [40] reported the dilatometric study of dense geopolymers, showing consistent shrinkage from room temperature to 800°C. They also calculated the thermal expansion coefficient, which is around $12\times10^{-6}/°C$, by measuring the expansion rate of post-heated samples in a second heating cycle. As the dilatometric study is performed at high temperature, it could reflect an overall small expansion when the shrinkage due to water loss is smaller than the thermal expansion. However, the much less dense GFC specimens studied here did not display such behavior after being cooled down to room temperature.

From 100°C to 800°C, both samples shrank to a larger extent. In combination with the results obtained through high temperature in-situ measurements [34, 35, 37], this can be divided into three sub-regions: in region I (100-300°C), a large shrinkage occurs mainly due to pore water

release from gels, also called 'capillary strain' [41]; region II (300-600°C), a relatively stable region where the few residual bound hydroxyl groups are lost without much volumetric change; and region III (600-800°C), which shows a large shrinkage to a 'sintering point' and then sometimes expansion. The temperature of the sintering point is affected by many factors, such as the solid materials, the calcium content, and the molar ratio of SiO_2/Na_2O used in the activator, which effectively defines geopolymer microstructure [42]. For example, the sintering point seems not to appear before 900°C if metakaolin is used as the raw material, and the samples are cured to maturity [31, 43]. However, for less-mature samples derived from fly ash, when SiO_2/Na_2O increases from 0 to 2.0, the sintering point shifts from >900°C to 700°C at a liquid/solid ratio of 0.125. An increased liquid/solid ratio also shifts the sintering point towards a lower temperature [35]. The liquid/solid ratio used in this study is 0.395, which may bring the sintering point lower than 800°C. However, it is noted that the 4% change observed here is still much less than would take place if the foamed structure of the GFC matrix was collapsing or densifying in a bulk sense, which means that the foamed nature of the material is clearly being retained.

Fig. 9 shows photographs of the samples before and after heating. The cross section of F5S0 does not show any macroscopic cracks, and only a few microcracks are observed on the surface after heating. However, there are visible cracks appearing on the cross section of F5S30 after exposure to 800°C, as shown in Fig. 9(d). This means that slag incorporation has changed the reaction products and their refractory behavior. This could be due to the presence of calcium, as reported previously for dense geopolymers [31, 37, 39]. Cracks were also observed on a cross section of solid inorganic polymer after heating at 900°C, when the material was synthesized with a high iron-content fly ash [44]. The presence of iron decreases the glass transition temperature (T_g) of the geopolymers, causing densification and shrinkage. This role

of iron, as a flux, was reported in the formation of coal ash slag (Al_2O_3-CaO-'FeO'-SiO_2) [45], in which a completely liquid phase was formed at lower temperature as FeO concentration increased. The previous study [38] also proposed that the crystallization at high temperature (700-800°C) may lead to the thermal expansion of fly ash geopolymers. Fig. 10 shows the XRD analysis of the GFCs before and after heating. As discussed above and in common with fly ash geopolymers in general, the reaction products in F5S0 are amorphous to semi-crystalline sodium aluminosilicates (N-A-S-(H)). These phases are different from the Ca-containing gel present in F5S30, and so may undergo different thermal transformation processes under firing temperatures. The major activation products present in both binders are amorphous, with a certain amount of unreacted mullite and quartz. When exposed to 800°C for 3 h, some of the amorphous phases in F5S0 crystallize into nepheline ($NaAlSiO_4$), which is often found in heated geopolymers [34, 46, 47]. In F5S30, the diffraction peaks attributed to nepheline are much more intense than in F5S0. Two other crystalline phases, åkermanite ($Ca_2Mg_{0.75}Al_{0.5}Si_{1.75}O_7$), associated with devitrification of remnant slag grains, and dehydrated Ca-substituted zeolite A ($CaNa_{11.44}Al_{11.21}Si_{11.59}O_{48}$) are observed. As noted above, the heating was only carried out at three temperatures (100, 400 and 800°C) in this study, so the expansion behaviour due to crystallization was not observable in detail. However, it is evident that the expansion, if any, could not compensate for the large shrinkage in the low temperature region.

Volumetric stability is a very important property for a fire resistant material. Dramatic shrinkage may cause cracks in a structure, or even structural collapse, even if each material component which comprises the structure is itself retaining satisfactory strength. The presence of calcium and iron is seen to be harmful to the volumetric stability of geopolymers under firing conditions. From this point of view, it is suggested to avoid calcium and iron bearing materials,

such as slag and high iron fly ash, in preparing geopolymers for use in refractory or high temperature applications.

3.4 Acoustic absorption

Fig. 11 shows the sound absorption properties of selected GFCs. The four samples tested provide a high degree of absorption for the low frequency sound waves, from 40 to 150 Hz. Slag substitution for 30% of the fly ash does not significantly change the absorption in the low frequency region, but increases the sound absorption at higher frequency, particularly at 800 to 1600 Hz. This is probably due to the changes in pore size, porosity and tortuosity introduced though the addition of the slag [48]. Increasing the thickness of the GFC specimens can increase the sound absorption in the low frequency region, to a greater extent than would be predicted simply from the fact that there is more material present through which the sound waves must be transmitted, but has insignificant effect at higher frequencies. The higher wavelength (lower frequency) sound is much more sensitive to the thickness of the material. Increasing the foam dosage from 5% to 10% seems to result in a material which is less effective for the absorption of low frequency sound, but more efficient for medium frequency sound, from 600 to 1000 Hz. Compared to the normal density PC concrete, which usually has an acoustic absorption coefficient <0.1 over the range 125 to 2000 Hz [49], GFC exhibits better acoustic absorption properties. The thin GFC specimens tested in this study have lower sound absorption in the medium to high frequency regions than ceramsite porous concrete, which has an average acoustic absorption coefficient >0.5 in this region [50]. However, any further increase in the thickness of the GFC material will increase its sound absorption.

4. Conclusions

Geopolymer foam concretes (GFCs) with a wide range of densities were successfully synthesized by mechanical mixing with preformed foam. Several properties of this material were investigated and reported for the first time:

(1) The compressive strength of GFC is notably influenced by slag substitution for fly ash. The 30% slag-containing GFC exhibits 28 d compressive strengths ranging from 3 to 48 MPa, depending on density. The relatively higher strength compared to PC foam concrete of equivalent density means that GFC may be able to be used for semi-structural to structural purposes.

(2) The thermal conductivities of the near-dried GFCs are in a range of 0.15 to 0.48 W/m·K when their demolded densities change from 720 to 1600 kg/m^3 (105°C oven-drying densities from 585 to 1370 kg/m^3) as the foam dosage decreases from 16% to 0. In this regard, GFC exhibits better thermal insulation property than normal PC foam concrete at the same density.

(3) The GFCs derived from alkali activation of low-calcium fly ash possess excellent strength retention after high temperature treatment; the compressive strength increases by 100% after exposure at 800°C. However, slag substitution for fly ash causes a large strength loss after heating, which is attributed to the loss of structural integrity of the calcium-rich components of the binder gel.

(4) Thin GFC specimens (20 - 25mm) exhibit an impressive acoustic absorption rate ($\alpha = 0.7$-1.0) in the low frequency region of 40 to 150 Hz. The average sound absorption of GFC is better than dense concrete, and could be equivalent to PC foam concrete.

Acknowledgement

References

[1] M.A. Othuman, Y.C. Wang, Elevated-temperature thermal properties of lightweight foamed concrete, Constr. Build. Mater. 25 (2) (2011) 705–716.

[2] F.K. Akthar, J.R.G. Evans, High porosity (>90%) cementitious foams, Cem. Concr. Res. 40 (2010) 352–358.

[3] O. Kreft, J. Hausmann, J. Hubálková, C.G. Aneziris, B. Straube, T. Schoch, Pore size distribution effects on the thermal conductivity of light weight autolaved aerated concrete, in 5th International Conference on Autoclaved Aerated Concrete, Bydgoscsz, Poland, 2011, pp. 257-264.

[4] Z. Zhang, J.L. Provis, A. Reid, H. Wang, Geopolymer foam concrete: An emerging material for sustainable construction, Constr. Build. Mater. 5 (2014) 113–127.

[5] J.L. Provis, S.A. Bernal, Geopolymers and related alkali-activated materials, Annu. Rev. Mater. Res., 44 (2014), 299-327,.

[6] P. Duxson, J.L. Provis, G.C. Lukey, J.S.J. van Deventer, The role of inorganic polymer technology in the development of 'green concrete', Cem. Concr. Res. 37 (2007) 1590–1597.

[7] R. Arellano Aguilar, O. Burciaga Díaz, J.I. Escalante García, Lightweight concretes of activated metakaolin-fly ash binders, with blast furnace slag aggregates, Constr. Build. Mater. 24 (2010) 1166–1175.

[8] D. Aldridge, Introduction to foamed concrete: what, why, how. In: Dhir RK, Newlands MD, McCarthy A (Eds). Use of foamed concrete in construction, London: Thomas Telford, 2005, pp. 1–14.

[9] E. Kamseu, B. Nait-Ali, M.C. Bignozzi, C. Leonelli, S. Rossignol, D.S. Smith, Bulk composition and microstructure dependence of effective thermal conductivity of porous inorganic polymer cements, J. Eur. Ceram. Soc. 32 (8) (2012) 1593–1603.

[10] E. Kamseu, B. Ceron, H. Tobias, E. Leonelli, M.C. Bignozzi, A. Muscio, A. Libbra, Insulating behavior of metakaolin-based geopolymer materials assess with heat flux meter and laser flash techniques, J. Therm. Anal. Calorim. 108 (3) (2011) 1189–1199.

[11] P. Duxson, G.C. Lukey, J.S.J. van Deventer, Thermal conductivity of metakaolin geopolymers used as a first approximation for determining gel interconnectivity, Ind. Eng. Chem. Res. 45 (23) (2006) 7781-7788.

[12] E. Prud'homme, P. Michaud, E. Joussein, C. Peyratout, A. Smith, S. Arrii-Clacens, J.M. Clacens, S. Rossignol, Silica fume as porogent agent in geo-materials at low temperature, J. Eur. Ceram. Soc. 30 (2010) 1641– 1648.

[13] J. Henon, A. Alzina, J. Absi, D.S. Smith, S. Rossignol, Porosity control of cold consolidated geomaterial foam: temperature effect, Ceram. Int. 38 (2012) 77–84.

[14] F. Gouny, F. Fouchal, P. Maillard, S. Rossignol, A geopolymer mortar for wood and earth structures. Constr. Build. Mater. 36 (2012) 188–195.

[15] Z. Zhang, H. Wang, A. Reid, T. Aravinthan, Effects of fly ash source and curing procedure on strength development of geopolymers. In: Incorporating Sustainable Practice in Mechanics of Structures and Materials, ACMSM 21, Melbourne, Australia, 2010. CRC Press, Taylor & Francis Group.

[16] M.M. Al Bakri Abdullah, K. Hussin, M. Bnhussain, K.N. Ismail, Z. Yahya, R.A. Razak, Fly ash-based geopolymer lightweight concrete using foaming agent, Int. J. Mol. Sci. 13 (6) (2012) 7186–7198.

[17] K. Brady, G. Watts, M.R. Jones, Specification for foamed concrete. Highways agency and TRL application guide AG 39, 2001.

[18] Y.S. Choy, L. Huang, C. Wang, Sound propagation in and low frequency noise absorption by helium-filled porous material, J. Acoust. Soc. Am. 126 (6) (2009) 3008–3019.

[19] N. Narayanan, K. Ramamurthy, Structure and properties of aerated concrete: a review. Cem. Concr. Compos. 22 (5) (2000) 321–329.

[20] F. Puertas, S. Martínez-Ramírez, S. Alonso, T. Vázquez, Alkali-activated fly ash / slag cement Strength behaviour and hydration products. Cem. Concr. Res. 30 (2000) 1625–1632.
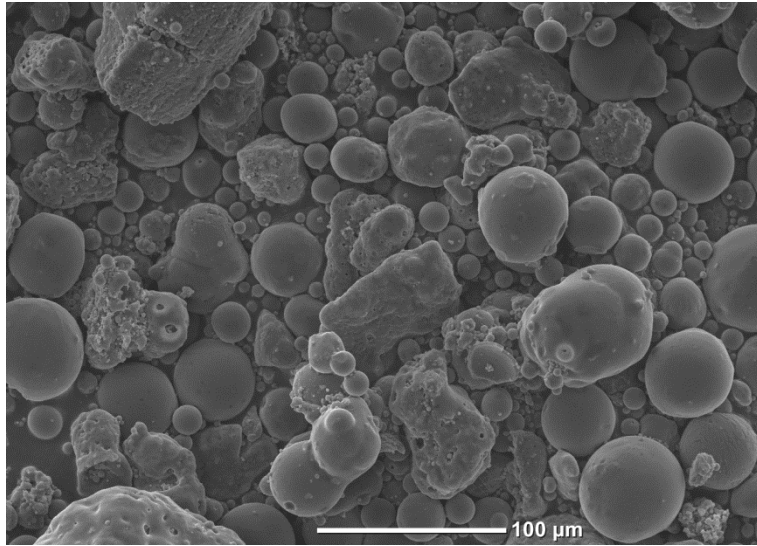
[21] S. Kumar, R. Kumar, S. Mehrotra, Influence of granulated blast furnace slag on the reaction, structure and properties of fly ash based geopolymer, J. Mater. Sci. 45 (3) (2010) 607–615.

[22] T. Yang, X. Yao, Z. Zhang, H. Wang, Mechanical property and structure of alkali-activated fly ash and slag blends. J. Sust. Cem.-Based Mater. 1 (4) (2012) 167–178.

[23] I. Ismail, S.A. Bernal, J.L. Provis, R. San Nicolas, D.G. Brice, A.R. Kilcullen, S. Hamdan, J.S.J. van Deventer, Influence of fly ash on the water and chloride permeability of alkali-activated slag mortars and concretes, Constr. Build. Mater. 48 (2013) 1187–1201.

[24] W.K.W. Lee, J.S.J. van Deventer, Effects of anions on the formation of aluminosilicate gel in geopolymers, Ind. Eng. Chem. Res. 41(18) (2002) 4550–4558.

[25] F. Winnefeld, A. Leemann, M. Lucuk, P. Svoboda, M. Neuroth, Assessment of phase formation in alkali activated low and high calcium fly ashes in building materials, Constr. Build. Mater. 24 (6) (2010) 1086–1093.

[26] E.K. Kunhanandan Nambiar, K. Ramamurthy, Influence of filler type on the properties of foam concrete, Cem. Concr. Compos. 28 (2006) 475–480.

[27] Z. Pan, F. Hiromi, W. Tionghuan, Preparation of high performance foamed concrete from cement, sand and mineral admixtures, J. Wuhan. Uni. Tech–Mater. Sci. Ed. 22 (2) (2007) 295–298.

[28] G. De Schutter, L. Taerwe. Specific heat and thermal diffusivity of hardening concrete. Mag. Concr. Res. 47 (172) (1995) 203–208.

[29] A. Fernández-Jiménez, A. Palomo, J.Y. Pastor, A. Martín, New cementitious materials based on alkali-activated fly ash: performance at high temperatures, J. Am. Ceram. Soc., 91 (10) (2008) 3308–3314.

[30] W.D.A. Rickard, R. Williams, J. Temuujin, A. van Riessen, Assessing the suitability of three Australian fly ashes as an aluminosilicate source for geopolymers in high temperature applications, Mater. Sci. Eng. A 528 (9) (2011) 3390–3397.

[31] S.A. Bernal, E.D. Rodríguez, R. Mejia de Gutiérrez, M. Gordillo, J.L. Provis, Mechanical and thermal characterisation of geopolymers based on silicate-activated metakaolin/slag blends, J Mater. Sci. 46 (16) (2011), 5477–5486.
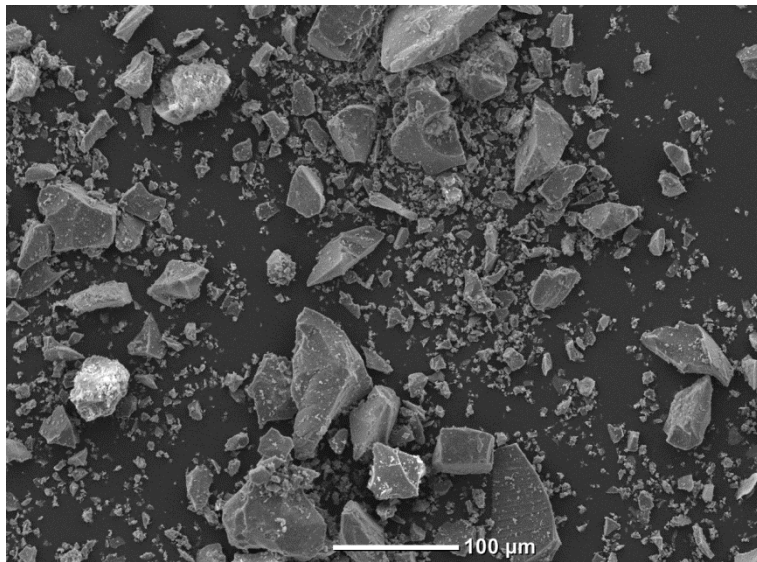
[32] L. Vickers, W.D.A. Rickard, A.van Riessen, Strategies to control the high temperature shrinkage of fly ash based geopolymers, Thermochim. Acta 580 (2014) 20–27.

[33] P. Hlaváček, V.Šmilauer, F.Škvára, L. Kopecký, R.Šulc, Inorganic foams made from alkali-activated fly ash: Mechanical, chemicaland physical properties, J. Eur. Ceram. Soc. 35 (2015) 703–709.

[34] J.L. Provis, R.M. Harrex, S.A. Bernal, P. Duxson, J.S.J. van Deventer, Dilatometry of geopolymers as a means of selecting desirable fly ash sources, J. Non-Cryst. Solids 358 (16) (2012) 1930-1937.

[35] J.L. Provis, C.Z. Yong, P. Duxson, J.S.J. van Deventer, Correlating mechanical and thermal properties of sodium silicate-fly ash geopolymers, Colloids Surfaces A 336 (1–3) (2009) 57–63.

[36] Z. Zhang, X. Yao, H. Zhu, Y. Chen, Role of water in the synthesis of calcined kaolin-based geopolymer. Appl. Clay Sci. 43 (2009) 218–223.

[37] K. Dombrowski, A. Buchwald, M. Weil, The influence of calcium content on the structure and thermal performance of fly ash based geopolymers, J. Mater. Sci. 42 (2007) 3033–3043.

[38] W.D.A. Rickard, A. van Riessen, P. Walls, Thermal character of geopolymers synthesized from Class F fly ash containing high concentrations of iron and alpha-quartz, Int. J. Appl. Ceram. Tech. 7(1) (2010) 81–88.

[39] A. Natali Murri, W.D.A. Rickard, M.C. Bignozzi, A. van Riessen, High temperature behaviour of ambient cured alkali-activated materials based on ladle slag, Cem. Concr. Res. 43 (2013) 51–61.

[40] P.N. Lemougna, K.J.D. MacKenzie, U.F. Chinje Melo, Synthesis and thermal properties of inorganic polymers (geopolymers) for structural and refractory applications from volcanic ash, Ceram. Int. 37 (8) (2011) 3011–3018.

[41] P. He, D. Jia, M. Wang, Y. Zhou, Thermal evolution and crystallization kinetics of potassium-based geopolymer, Ceram. Int. 37(1) (2011) 59–63.

[42] P. Duxson, J.L. Provis, G.C. Lukey, S.W. Mallicoat, W.M. Kriven, J.S.J van Deventer, Understanding the relationship between geopolymer composition, microstructure and mechanical properties, Colloids Surfaces A, 269(1-3) (2005) 47–58.

[43] P. Duxson, G.C. Lukey, J.S.J. van Deventer, Thermal evolution of metakaolin geopolymers: Part 1-Physical evolution, J. Non-Cryst. Solids. 352 (52-54) (2006) 5541–5555.

[44] W.D.A. Rickard, A. van Riessen, P. Walls, Thermal character of geopolymers synthesized from Class F fly ash containing high concentrations of iron and alpha-quartz, Int. J. Appl. Ceram. Tech. 7(1) (2010) 81–88.

[45] A. Kondratiev, E. Jak, Predicting coal ash slag flow characteristics (viscosity model for the Al_2O_3-CaO-'FeO'-SiO_2 system). Fuel 80 (2001) 1989–2000.

[46] A.M. Rashad, S.R. Zeedan, The effect of activator concentration on the residual strength of alkali-activated fly ash pastes subjected to thermal load, Constr. Build. Mater. 25(7) (2011) 3098–3107.

[47] C. Kuenzel, L.M. Grover, L. Vandeperre, A.R. Boccaccini, C.R. Cheeseman, Production of nepheline/quartz ceramics from geopolymer mortars, J. Eur. Ceram. Soc. 33(2) (2013) 251–258.

[48] J.L. Provis, R.J. Myers, C.E. White, V. Rose, J.S.J. van Deventer, X-ray microtomography shows pore structure and tortuosity in alkali-activated binders, Cem. Concr. Res. 42 (6) (2012) 855-864.

[49] V. Tiwari, A. Shukla, A. Bose, Acoustic properties of cenosphere reinforced cement and asphalt concrete, Appl. Acous. 65 (2004) 263–275.

[50] X.Y. Luo, W.F. Li, X.L. Jin, L.K. Zeng, Effects of porosity and pore size on sound absorption characteristic of Ceramsite porous material, J. Chin. Ceram. Soc. 39 (1) (2011) 158–163.

(a)

(b)
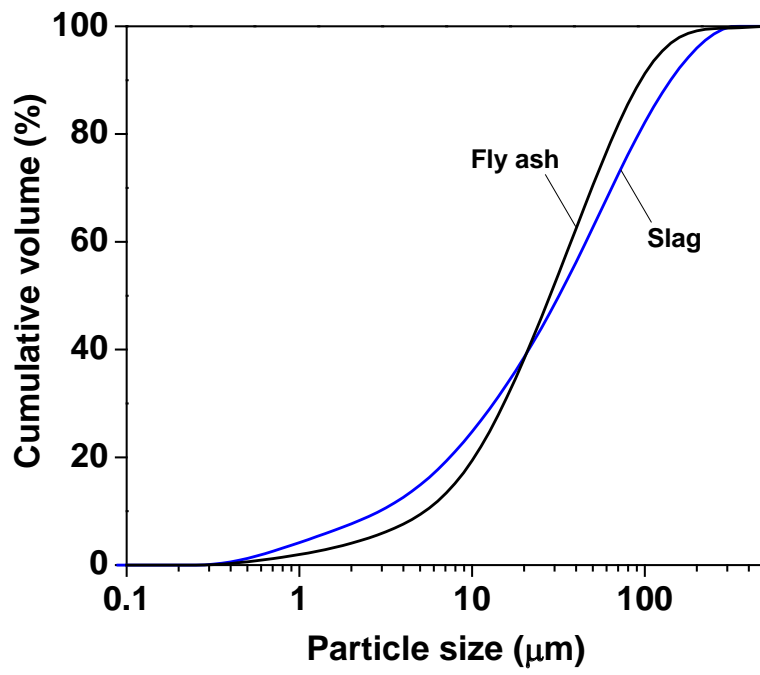
Fig. 1. SEM images of (a) fly ash and (b) slag.

Fig. 2. Cumulative particle size distributions of fly ash and slag.
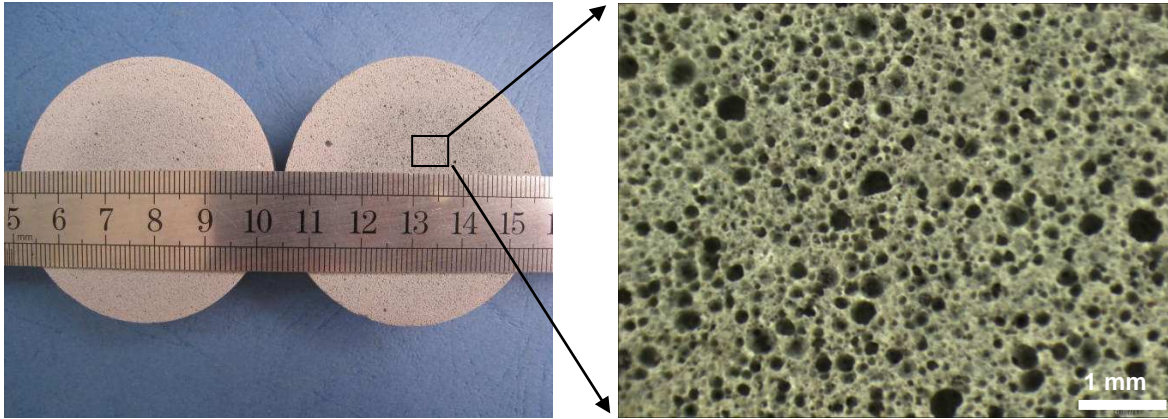
Fig. 3. GFC slices used for thermal conductivity testing. The optical micrograph shows the pore structure.
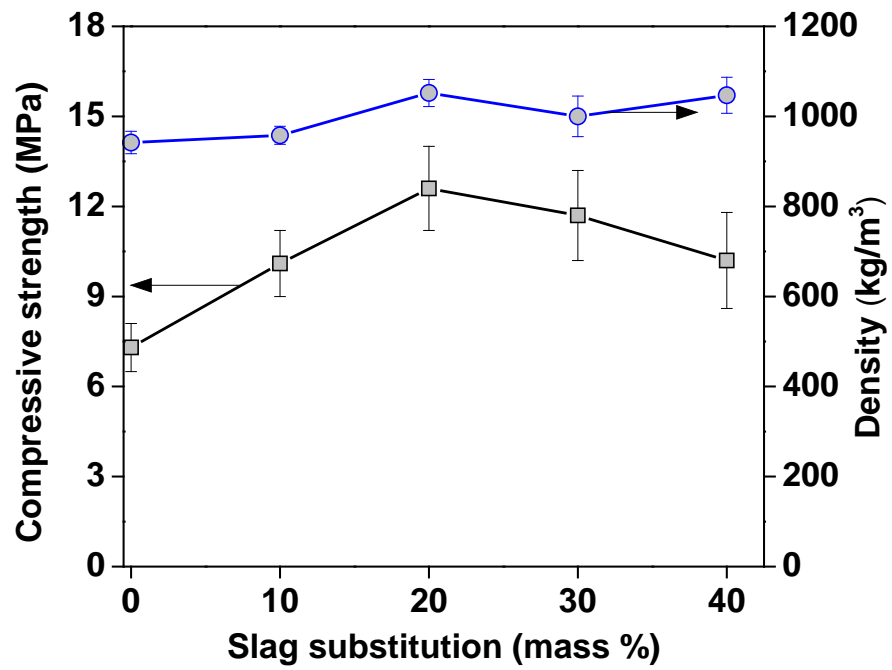
Fig.4. Compressive strength and demolded density of GFC as a function of slag substitution for fly ash.
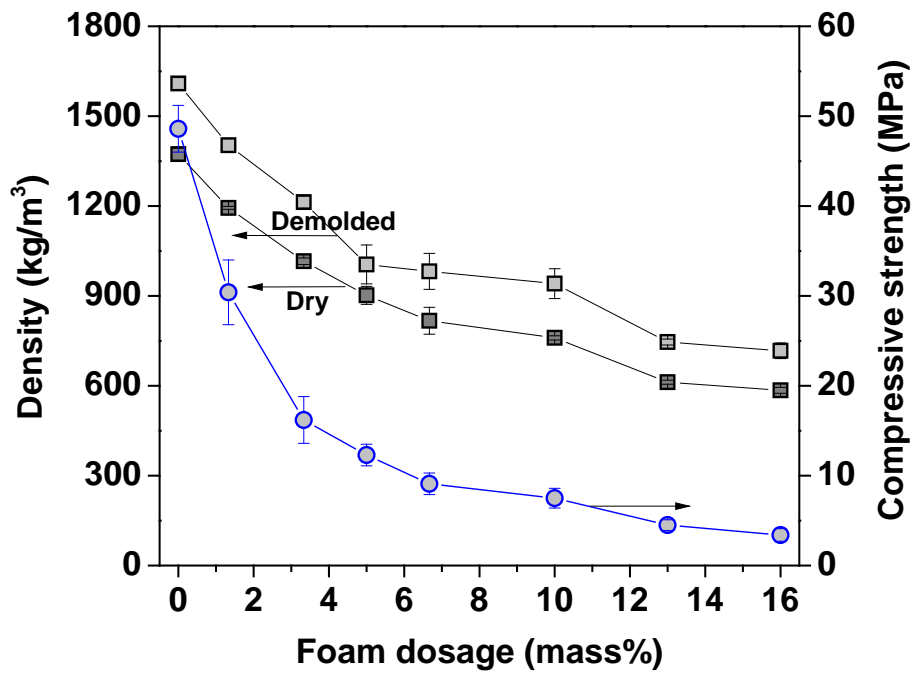
Fig.5. Compressive strength, demolded density and dry density of GFC as a function of foam dosage (in terms of mass ratio of solid materials). The slag substitution is constant at 30%.
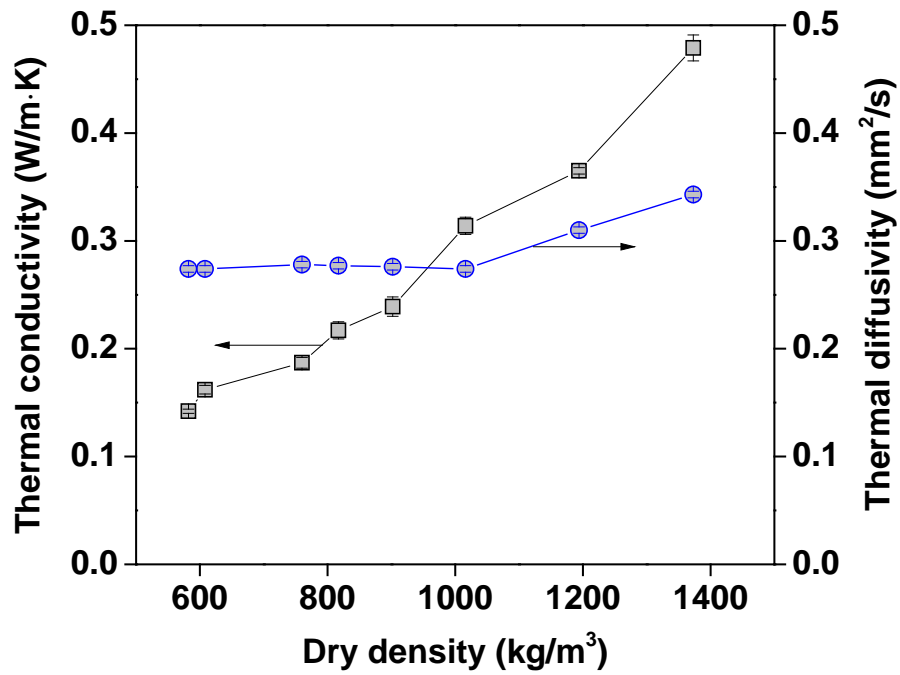
Fig.6. Thermal conductivity of GFC as a function of foam dosage. Error bars show the standard deviation between four replicate tests.
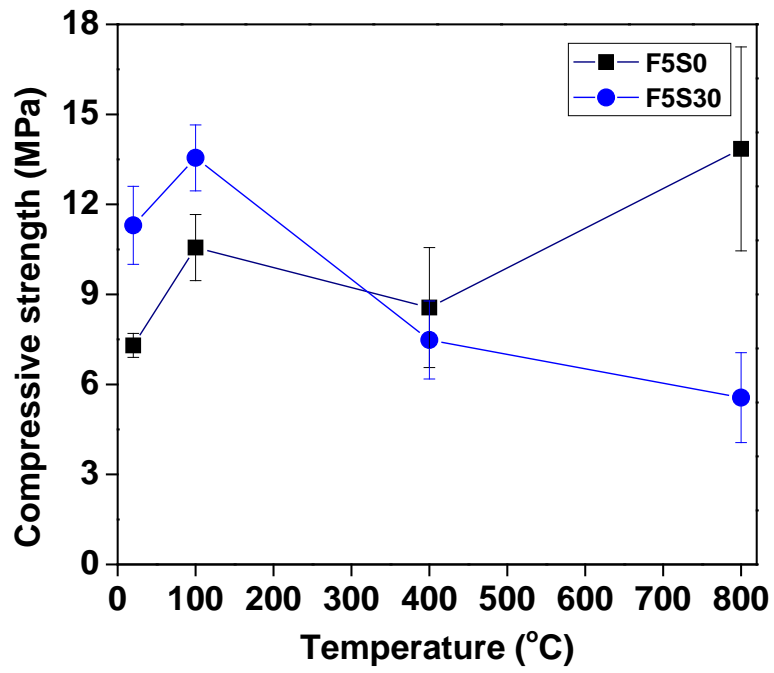
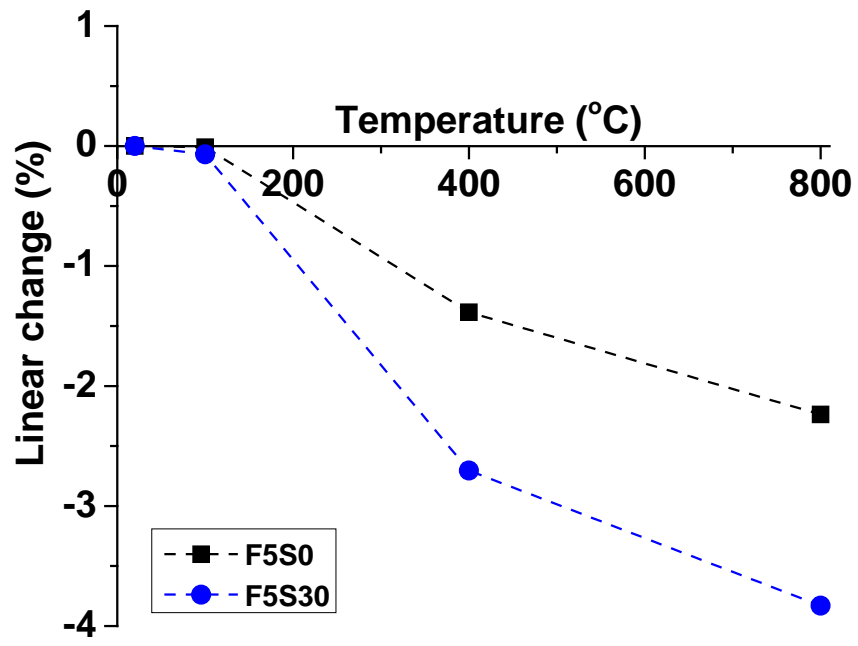Fig.7. Compressive strengths of GFCs F5S0 and F5S30 after exposure to different temperatures.

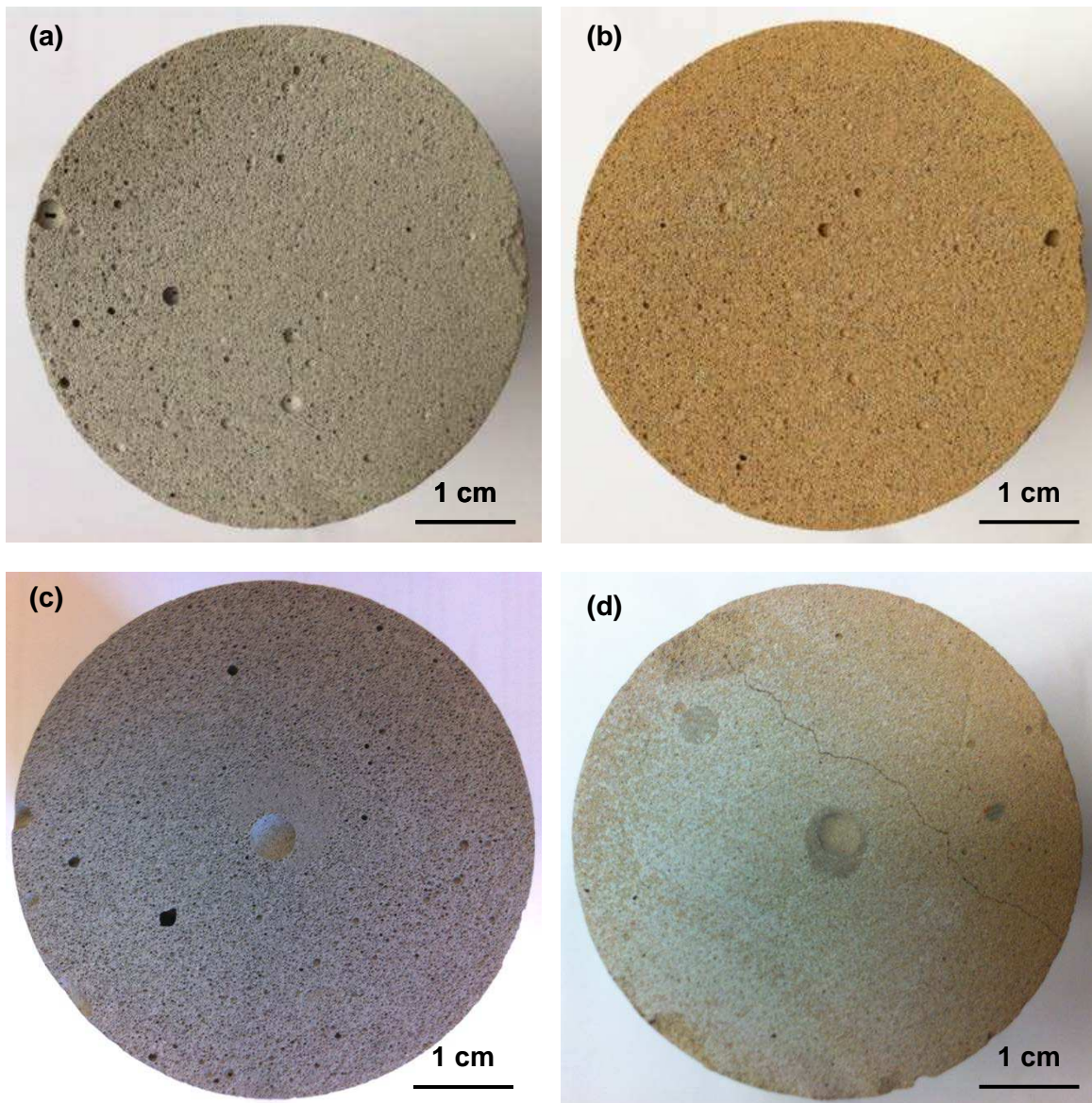Fig.9. Linear shrinkage of GFC after heating.

Fig.9. Cross-section of GFC specimens: (a) F5S0 before; (b) F5S0 after; (c) F5S30 before; and (d) after 800°C exposure.
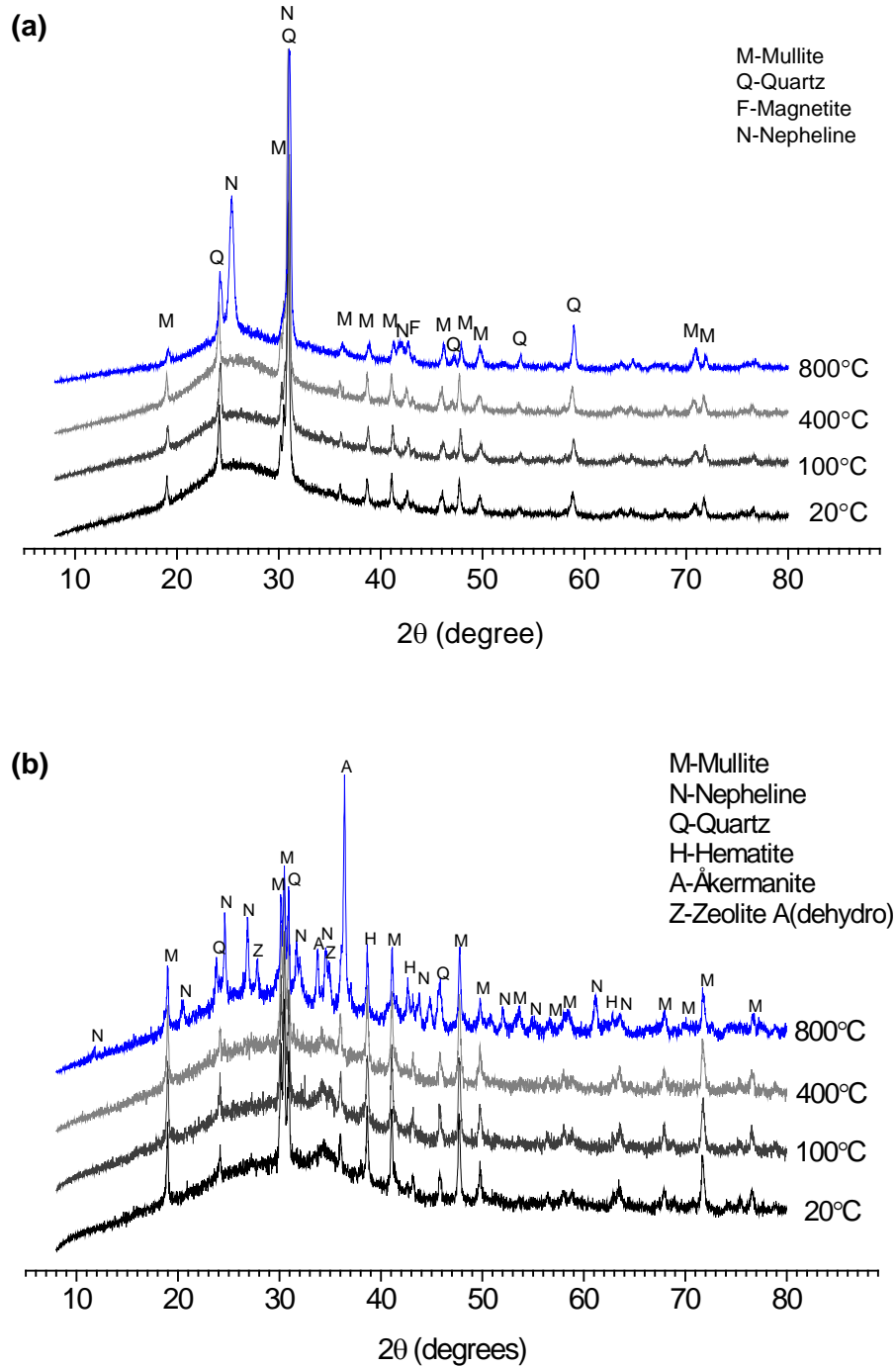
Fig. 10. XRD patterns of GFCs before and after high temperature exposure: (a) F5S0; (b) F5S30. Phases identified: mullite, $Al_{4.8}Si_{1.2}O_{9.5}$; nepheline, $NaAlSiO_4$; åkermanite, $Ca_2Mg_{0.75}Al_{0.5}Si_{1.75}O_7$; dehydrated zeolite (Ca,Na)-A, $CaNa_{11.44}Al_{11.21}Si_{11.59}O_{48}$.
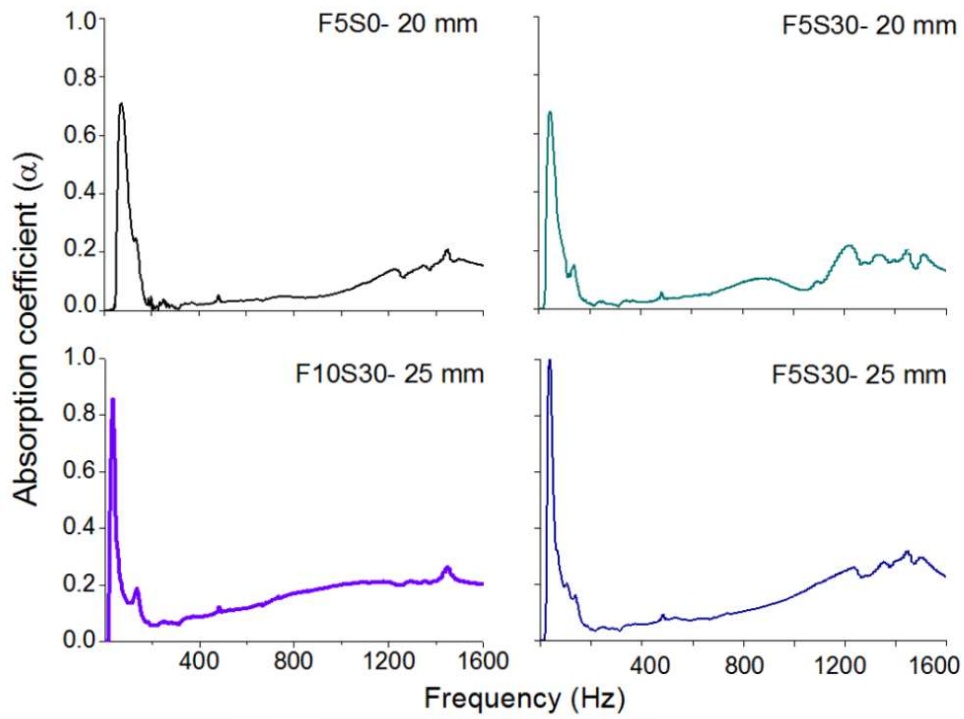
Fig. 11. Acoustic absorption spectra for selected GFCs with thicknesses of 20 mm and 25 mm, as marked.

Figure 1	SEM images of (a) fly ash and (b) slag.
Figure 2	Cumulative particle size distributions of fly ash and slag.
Figure 3	GFC slices used for thermal conductivity testing. The optical micrograph shows the pore structure.
Figure 4	Compressive strength and demolded density of GFC as a function of slag substitution for fly ash.
Figure 5	Compressive strength, demolded density and dry density of GFC as a function of foam dosage (in terms of mass ratio of solid materials). The slag substitution is constant at 30%.
Figure 6	Thermal conductivity of GFC as a function of foam dosage. Error bars show the standard deviation between four replicate tests.
Figure 7	Compressive strengths of GFCs F5S0 and F5S30 after exposure to different temperatures.
Figure 8	Linear shrinkage of GFC after heating.
Figure 9	Cross-section of GFC specimens: (a) F5S0 before; (b) F5S0 after; (c) F5S30 before; and (d) after 800°C exposure.
Figure 10	XRD patterns of GFCs before and after high temperature exposure: (a) F5S0; (b) F5S30. Phases identified: mullite, $Al_{4.8}Si_{1.2}O_{9.5}$; nepheline, $NaAlSiO_4$; åkermanite, $Ca_2Mg_{0.75}Al_{0.5}Si_{1.75}O_7$; dehydrated zeolite (Ca,Na)-A, $CaNa_{11.44}Al_{11.21}Si_{11.59}O_{48}$.
Figure 11	Acoustic absorption spectra for selected GFCs with thicknesses of 20 mm and 25 mm, as marked.

Table 1. Compositions of fly ash and slag as determined by XRF, wt.%. LOI is loss on ignition at 1000°C.

	SiO_2	Al_2O_3	CaO	MgO	K_2O	Na_2O	Fe_2O_3	P_2O_5	SO_3	TiO_2	LOI
Fly ash	72.1	24.7	0.1	0.2	0.5	≤0.1	1.2	≤0.1	≤0.1	1.4	0.4
Slag	33.3	14.6	41.7	6.1	0.3	0.2	0.8	0.2	0.6	0.6	0.5

Table 2. Mix proportions of the GFCs.

Mixture	Fly ash (g)	Slag (g)	NaOH solution, 12 M (g)	Sodium silicate, Ms = 2.0 (g)	Water (g)	Foam (g)
F5S0	100	0	15.5	24	8	5
F5S10	90	10	15.5	24	7	5
F5S20	80	20	15.5	24	6.5	5
F5S30	70	30	15.5	24	6	5
F5S40	60	40	15.5	24	6	5
F0S30	70	30	15.5	24	10	0
F1.3S30	70	30	15.5	24	10	1.3
F3.3S30	70	30	15.5	24	8	3.3
F6.7S30	70	30	15.5	24	4.5	6.7
F10S30	70	30	15.5	24	3	10
F13S30	70	30	15.5	24	1.5	13
F16S30	70	30	15.5	24	0	16